

# Subharmonic instabilities in Kerr microcombs

GUOPING LIN,<sup>1</sup> FENGYU LIU,<sup>2</sup> AURÉLIEN COILLET,<sup>3</sup> DAMIÀ GOMILA,<sup>4</sup> CURTIS R. MENYUK,<sup>5</sup> AND YANNE K. CHEMBO<sup>2,\*</sup>

<sup>1</sup>Ministry of Industry and Information Technology Key Lab of Micro-Nano Optoelectronic Information System, School of Science, Harbin Institute of Technology, Shenzhen 518055, China

<sup>2</sup>Department of Electrical and Computer Engineering & Institute for Research in Electronics and Applied Physics (IREAP), University of Maryland, 8279 Paint Branch Dr., College Park, Maryland 20742, USA

<sup>3</sup>Laboratoire Interdisciplinaire Carnot Bourgogne [CNRS UMR6303], Univ. Bourgogne-Franche-Comté, 9 Avenue A. Savary, 21078 Dijon, France

<sup>4</sup>Instituto de Física Interdisciplinar y Sistemas Complejos, IFISC (CSIC-UIB), Campus Universitat de les Illes Balears, E-07122 Palma de Mallorca, Spain

<sup>5</sup>Department of Computer Science and Electrical Engineering, University of Maryland Baltimore County, 1000 Hilltop Circle, Baltimore, Maryland 21250, USA

\*Corresponding author: ykchembo@umd.edu

Received 27 September 2022; revised 26 November 2022; accepted 26 November 2022; posted 28 November 2022; published 18 January 2023

**We report experimental observation of subharmonic mode excitation in primary Kerr optical frequency combs generated using crystalline whispering-gallery mode resonators. We show that the subcombs can be controlled and span a single or multiple free spectral ranges around the primary comb modes. In the spatial domain, the resulting multiscale combs correspond to an amplitude modulation of intracavity roll patterns. We perform a theoretical analysis based on eigenvalue decomposition that evidences the mechanism leading to the excitation of these combs.** © 2023 Optica Publishing Group

<https://doi.org/10.1364/OL.476647>

Optical frequency combs have played a role of great importance in the field of metrology and spectroscopy in recent years. Initially, the generation of these combs was typically based on mode-locked lasers, but a novel alternative way to generate using optical resonators was proposed a few years ago [1]. These optical cavities feature whispering-gallery modes (WGMs) with high quality ( $Q$ ) factors and small mode volumes, so that stimulated four-wave mixing can occur at a relatively low threshold pump power. Under optimal conditions, a resonant single frequency continuous wave pump laser can trigger the generation of an equidistant frequency comb in the spectral domain, which is generally referred to as a Kerr optical frequency comb. Potential applications for these combs include coherent optical communications [2,3], spectroscopy [4], or low phase noise microwave generation [5].

Kerr optical frequency combs can be of various types, depending on the nature of the underlying intracavity dissipative pattern, which can be extended (Turing rolls) or localized (bright, dark, or breather solitons). The extended patterns are also known as optical parametric oscillations or cnoidal waves, and they correspond to a set of equidistant rolls (or pulses) distributed along the azimuthal direction of the resonator. Turing rolls are

excited via modulation instability and in the Fourier domain, the corresponding spectra are known as primary combs.

It is important to note that these combs are excited harmonically, i.e., the comb lines appear as multiples of the main offset frequency from the pumped mode, which is itself an integer multiple of the free spectral range (FSR). Spectra of Kerr optical frequency combs have been extensively studied at both the experimental and theoretical levels, and are quite well understood today [4,6–12]. However, the excitation of subharmonic combs can be observed via parametric seeding [13] or dual pumping [14]. However, it is counter-intuitive to assume that a Kerr-nonlinear resonator pumped with a single resonant laser can output subharmonic comb lines (or subcombs), which are made of modes with a reduced azimuthal order that is a rational proportion of the main offset line (the ratio being of the kind  $p/q$  with  $p$  and  $q$  being positive integers).

In this Letter, we report on experimental subharmonic comb generation emerging as a bifurcation from primary combs originating from a crystalline whispering-gallery mode disk resonator, without using parametric seeding or a multi-pump source. We show that the frequency spacing of the subcomb can be tuned to up to 7 FSR, and the comb beat signal confirms their equidistance. An eigenvalue analysis is developed to explain the origin of this phenomenology.

The experimental setup is sketched in Fig. 1(a). A magnesium fluoride ( $\text{MgF}_2$ ) disk resonator with a  $Q$ -factor above one billion at 1550 nm and a diameter slightly less than 12 mm is used for the generation of the Kerr optical frequency combs. It is fabricated using the mechanical polishing method on the surface of its spherical rim [15]. To efficiently excite optical WGMs, a low-loss single-mode tapered fiber coupler is made using the heat-and-pull method with a butane flame [16]. The fiber-cavity coupling setup picture is given in the inset of Fig. 1(a). A tunable single frequency external cavity diode laser is used as the pump laser. A fiber polarization controller can then optimize the polarization matching condition between the

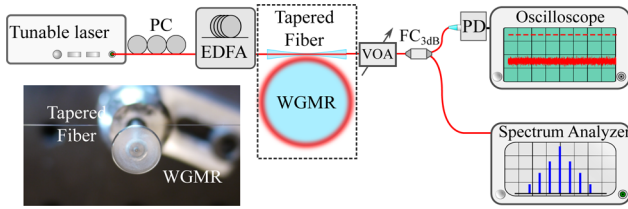


**Fig. 1.** Schematic of the experimental setup. PC, fiber polarization controller; EDFA, erbium-doped fiber amplifier; VOA, variable fiber optical attenuator; FC<sub>3dB</sub>, 1 × 2 50:50 fiber coupler; PD, photodetector.

laser and the cavity modes. Since the cavity dispersion plays an important role in the Kerr comb generation, it is necessary to excite various WGMs with either small or large mode volumes for exploring the rich Kerr comb dynamics in a single resonator. To reach the parametric oscillation threshold in such a centimeter-scale cavity, we use an erbium-doped fiber amplifier (EDFA) to get sufficient continuous pump power up to 200 mW. The output port of the taper is connected to a variable fiber attenuator and then sent to a 1 × 2 fiber coupler. This setup permits to monitor simultaneously the spectrum of the comb using a high resolution spectrum analyzer (Apex 2440B with resolution down to 5 MHz) and the transmitted light power in the photodetector (PD). A fast photodiode is also used for monitoring the beatnote in the RF domain (not illustrated here).

The laser wavelength is tuned step by step via temperature variation. To study the stable comb spectra, we stabilize the laser wavelength to the optical resonances using self-thermal locking [17]. In the MgF<sub>2</sub> WGM resonator, both the thermo-refractive and thermal expansion coefficients are positive. Correspondingly, the heat generated by an absorption portion of the intracavity pump shifts the resonance frequency in the same direction (redshift) for these two effects. Therefore, the pump laser with constant frequency and sufficient pump power can continuously excite the optical mode without causing a self-pulsing effect that is usually observed in crystals with opposite signs of the two thermal coefficients [18].

Here, we focus on the excitation of primary combs with subcomb lines. Figure 2 shows the optical spectra of five combs obtained by exciting different transverse optical modes in the cavity. We measure the single FSR value of 5.9 GHz by monitoring the beatnote frequency of a single FSR comb in a fast photodetector. The primary comb spacings for these five combs are found to be 50 FSR, 38 FSR, 42 FSR, 84 FSR, and 45 FSR, respectively. This spacing difference results from the cavity dispersion variation among different families of WGMs [19]. However, the dispersion profile for each of these mode families has not been characterized experimentally, so that the exact value of group-velocity dispersion in each case remains unknown. Interestingly, we observe the subcomb lines with different frequency spacings around the primary comb as we detune the laser from the resonance frequency of the pumped mode. The experimental combs are displayed in Fig. 2. One can clearly see in the inset of Fig. 2(b) that the subcomb lines have a single FSR spacing, while the spacings are 2 FSR and 3 FSR in Figs. 2(c) and 2(d), respectively. In this experiment, subcomb lines in the primary comb regime with the frequency spacing up to 7 FSR are observed as well [Fig. 2(e)]. Figure 3 shows the corresponding beatnote spectra in the RF domain by using

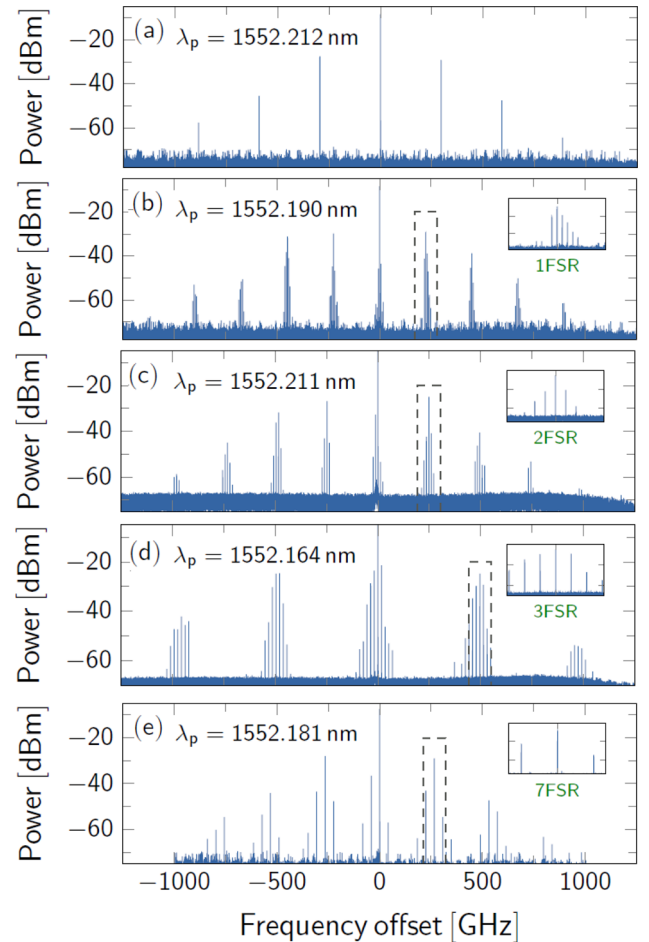


**Fig. 2.** Five experimental Kerr comb spectra (from top to bottom): pure primary comb, primary combs with 1-FSR, 2-FSR, 3-FSR, and 7-FSR-spaced subcomb lines. The primary comb spacing number  $m$  is 50, 38, 42, 84, and 45, respectively. Note that the single FSR is 5.9 GHz and that the resonant modes for the pump laser are different. Insets display a zoom of the spectra of the highlighted zones.

a fast photodiode and a electrical spectrum analyzer. One can see that we can recover single-FSR (5.9 GHz) and double-FSR (11.8 GHz) beatnotes.

The origin of these subharmonic excitations can be investigated theoretically via an eigenvalue analysis [20–22]. We start with the coupled mode equations that govern the dynamics of Kerr optical frequency combs up to second-order dispersion, following

$$\begin{aligned} \dot{\mathcal{E}}_l = & -\kappa \mathcal{E}_l + i \left[ \sigma - \frac{1}{2} \zeta_2 l^2 \right] \mathcal{E}_l \\ & + i v_g \gamma \sum_{m,n,p} \delta(m-n+p-l) \mathcal{E}_m \mathcal{E}_n^* \mathcal{E}_p \\ & + \delta(l) \sqrt{2\kappa_c/T_R} \sqrt{P_L}, \end{aligned} \quad (1)$$

where the complex-valued modal field envelopes  $\mathcal{E}_l$  are normalized such that their modulus square is the modal power (in Watts), while  $l$  stands for the reduced azimuthal eigennumber (with  $l = 0$  representing the pumped mode, with the sidemodes expanding as  $l = \pm 1, \pm 2, \dots$ ). The parameters of the equation are the round trip period  $T_R$ , half-linewidth of the resonator  $\kappa$ ,

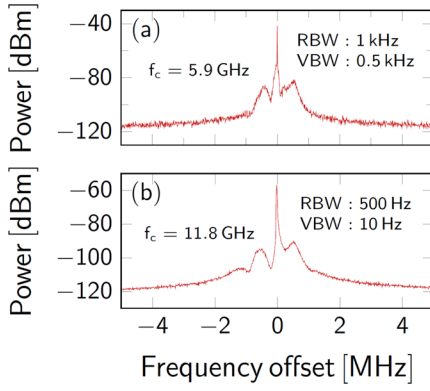


**Fig. 3.** Experimental radio frequency spectra obtained after photodetection of the subcombs. (a) Spectrum of the single-FSR beatnote (5.9 GHz) for the comb of Fig. 2(b). (b) Spectrum of the double-FSR beatnote (11.8 GHz) for the comb of Fig. 2(c).

half-linewidth for the through port  $\kappa_e$ , the detuning  $\sigma$  between the laser and the pumped angular frequencies, the group-velocity dispersion  $\zeta_2$  (in units of rad/s), the group velocity  $v_g$ , the non-linear parameter  $\gamma$  (in units of  $\text{W}^{-1}\text{m}^{-1}$ ), and the power of the laser  $P_L$  (in units of Watts).

In our computational procedure, for Turing patterns of order  $L$ , we only keep  $N$  modes in each side and it contains  $M$  excited modes separately. We proceed with a numerical simulation of the full model based on the split-step Fourier algorithm, and once a stationary solution  $E = (\mathcal{E}_{-N}, \dots, \mathcal{E}_N)$  is found, the perturbation can be written with the stationary solution as

$\delta\mathcal{E} = (\delta\mathcal{E}_{-N}, \dots, \delta\mathcal{E}_N)$ . Then, we linearize Eq. (1) about the stationary solution as

$$\begin{bmatrix} \delta\dot{\mathcal{E}} \\ \delta\dot{\mathcal{E}}^* \end{bmatrix} = \mathbf{J} \begin{bmatrix} \delta\mathcal{E} \\ \delta\mathcal{E}^* \end{bmatrix} \quad (2)$$

with

$$\mathbf{J} = \begin{bmatrix} \mathbf{R} & \mathbf{S} \\ \mathbf{S}^* & \mathbf{R}^* \end{bmatrix}. \quad (3)$$

The complex-valued Jacobian matrix  $\mathbf{J}$  is explicitly defined as

$$\begin{aligned} \mathcal{R}_{lp} = & \left[ -\kappa + i(\sigma - \frac{\zeta_2}{2} l^2) \right] \delta(p-l) \\ & + 2iv_g \gamma \sum_{m,n} \delta(m-n+p-l) \mathcal{E}_m \mathcal{E}_n^*, \end{aligned} \quad (4)$$

$$\mathcal{S}_{lp} = iv_g \gamma \sum_{m,n} \delta(m+n-p-l) \mathcal{E}_m \mathcal{E}_n. \quad (5)$$

This Jacobian is block diagonal with  $L/2 + 1$  boxes if  $L$  is even, and  $(L+1)/2$  boxes if  $L$  is odd. For convenience, we rewrite it to make the  $q$ th block  $\mathbf{J}_q$  correspond to the perturbation:

$$\delta\mathcal{E}^{(q)} = (\delta\mathcal{E}_{-ML-q}, \dots, \delta\mathcal{E}_{ML-q}, \delta\mathcal{E}_{-ML+q}, \dots, \delta\mathcal{E}_{ML+q}), \quad (6)$$

which is sometimes referred to as a “Bloch mode” [23]. The block Jacobian  $\mathbf{J}_q$  can be explicitly written as

$$\mathbf{J}_q = \begin{bmatrix} \mathbf{R}_q & \mathbf{S}_q \\ \mathbf{S}_q^* & \mathbf{R}_q^* \end{bmatrix}, \quad (7)$$

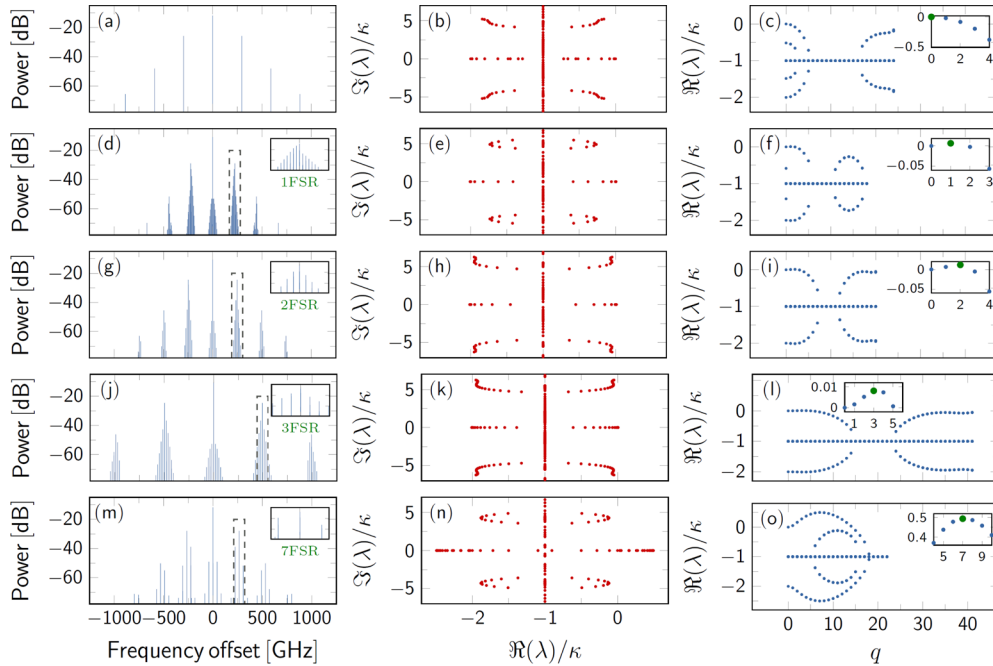


**Fig. 4.** (a),(d),(g),(j),(m) Five types of Kerr comb spectra snapshots of the output fields, in correspondence with the experimental spectra of Fig. 2, with the same subcomb structures. Quality factor of the through port is set to  $Q_e = Q/4$ , and the nonlinear parameter is set to  $\gamma = 1.0 \text{ W}^{-1}\text{km}^{-1}$ . From top to bottom, the detuning for each case is  $2\kappa$ ,  $2.3\kappa$ ,  $1.8\kappa$ ,  $1.83\kappa$ , and  $0.55\kappa$ , respectively, and the second-order dispersion  $\zeta_2$  is set to  $-0.0037$ ,  $-0.0073$ ,  $-0.0060$ ,  $-0.0015$ , and  $-0.0055$  in units of  $\kappa/v_g\omega_R^2$ . Pump power is set to 75, 90, 100, 100, and 75 mW. (b),(e),(h),(k),(n) Eigenvalues of the solution in a complex plane. (c),(f),(i),(l),(o) Real part of the eigenvalues plotted as a function of the wavenumber  $q$  of the Bloch modes. The solution is unstable when the real part of one of them becomes positive, and the eigenvalue with the largest positive real part corresponds to the order of the subcomb.

where

$$\mathbf{R}_q = \begin{bmatrix} \mathbf{U}_q & 0 \\ 0 & \mathbf{V}_q \end{bmatrix} \text{ and } \mathbf{S}_q = \begin{bmatrix} 0 & \mathbf{W}_q \\ \mathbf{W}_q^* & 0 \end{bmatrix} \quad (8)$$

are block matrices of order  $(4M + 2)$  for  $q \neq 0$  and  $q \neq L/2$ , with complex-valued elements

$$\mathcal{U}_{lp}^{(q)} = \mathcal{R}_{lL-q, pL-q}, \quad (9)$$

$$\mathcal{V}_{lp}^{(q)} = \mathcal{R}_{lL+q, pL+q}, \quad (10)$$

$$\mathcal{W}_{lp}^{(q)} = \mathcal{S}_{lL+q, pL-q} = \mathcal{S}_{lL-q, pL+q}. \quad (11)$$

For  $q = 0$  or  $q = L/2$ , we find that  $\mathbf{U}_q$  and  $\mathbf{V}_q$  are identical, so that  $\mathbf{R}_q$  and  $\mathbf{S}_q$  are matrices of order  $(2M + 1)$  or  $(2M + 2)$ , with  $\mathbf{R}_q = \mathbf{U}_q$  and  $\mathbf{S}_q = \mathbf{W}_q$ . The stability of the stationary solution can be determined by calculating the real parts of the eigenvalues. If the real part of any of the eigenvalues is positive, the solution is unstable. The results of this eigenvalue analysis are presented in the left column of Fig. 4, and they confirm that the subcombs originate from the most unstable Bloch mode, i.e., the one with the largest positive real part. In fact, the modulated patterns arising from this instability are typically unstable and can be observed as transients. When a pattern becomes unstable, it gets modulated by the growth of small-wavenumber perturbations. If the solution is decomposed as the modulus and phase, the small-wavenumber modulations correspond to variations of the phase with a long spatial scale. The dynamics of the modulus is relaxational, i.e., it has negative eigenvalues and can be adiabatically eliminated, while the dynamics of the phase is diffusive with significantly slower dynamics. As a consequence, the transients persist for a long time before the small-wavenumber modulations are smoothed out. However, the modulation can also be eventually stabilized by other intracavity nonlinear effects.

In conclusion, we have investigated the generation of subharmonic comb lines when ultrahigh- $Q$  WGM resonators are excited by a resonant continuous wave laser. We have shown that subcombs with various FSR spacings can be excited experimentally. These combs correspond to amplitude-modulated Turing rolls inside the optical cavity. We have also performed a theoretical analysis that enabled us to unveil that the origin of these additional comb lines is a subharmonic bifurcation leading to the excitation of a Bloch mode. Further research will be devoted to the interaction of this instability with other nonlinearities in the optical resonator [24].

**Funding.** European Research Council (278616); Air Force Office of Scientific Research (FA9550-20-1-0357).

**Acknowledgment.** This research was funded by the European Research Council (ERC Grant 278616) and by the Air Force Office of Scientific Research (AFOSR Grant FA9550-20-1-0357).

**Disclosures.** The authors declare that there are no conflicts of interest related to this paper.

**Data availability.** Data underlying the results presented in this paper are not publicly available at this time but may be obtained from the authors upon reasonable request.

## REFERENCES

- P. Del'Haye, A. Schliesser, O. Arcizet, T. Wilken, R. Holzwarth, and T. J. Kippenberg, *Nature* **450**, 1214 (2007).
- J. Pfeifle, V. Brasch, M. Lauermaun, Y. Yu, D. Wegner, T. Herr, K. Hartinger, P. Schindler, J. Li, D. Hillerkuss, R. Schmogrow, C. Weimann, R. Holzwarth, W. Freude, J. Leuthold, T. J. Kippenberg, and C. Koos, *Nat. Photonics* **8**, 375 (2014).
- J. Pfeifle, A. Coillet, R. Henriet, K. Saleh, P. Schindler, C. Weimann, W. Freude, I. V. Balakireva, L. Larger, C. Koos, W. Freude, I. V. Balakireva, L. Larger, C. Koos, and Y. K. Chembo, *Phys. Rev. Lett.* **114**, 093902 (2015).
- M.-G. Suh, Q.-F. Yang, K. Y. Yang, X. Yi, and K. J. Vahala, *Science* **354**, 600 (2016).
- W. Liang, D. Eliyahu, V. S. Ilchenko, A. A. Savchenkov, A. B. Matsko, D. Seidel, and L. Maleki, *Nat. Commun.* **6**, 7957 (2015).
- A. Pasquazi, M. Peccianti, L. Razzari, D. J. Moss, S. Coen, M. Erkintalo, Y. K. Chembo, T. Hansson, S. Wabnitz, P. Del'Haye, X. Xue, A. M. Weiner, and R. Morandotti, *Phys. Rep.* **729**, 1 (2018).
- T. Herr, V. Brasch, J. D. Jost, C. Y. Wang, N. M. Kondratiev, M. L. Gorodetsky, and T. J. Kippenberg, *Nat. Photonics* **8**, 145 (2014).
- X. Yi, Q.-F. Yang, K. Y. Yang, M.-G. Suh, and K. Vahala, *Optica* **2**, 1078 (2015).
- V. Brasch, M. Geiselmann, T. Herr, G. Lihachev, M. H. Pfeiffer, M. L. Gorodetsky, and T. J. Kippenberg, *Science* **351**, 357 (2016).
- C. Bao, J. A. Jaramillo-Villegas, Y. Xuan, D. E. Leaird, M. Qi, and A. M. Weiner, *Phys. Rev. Lett.* **117**, 163901 (2016).
- M. Yu, J. K. Jang, Y. Okawachi, A. G. Griffith, K. Luke, S. A. Miller, X. Ji, M. Lipson, and A. L. Gaeta, *Nat. Commun.* **8**, 14569 (2017).
- S.-W. Huang, J. Yang, S.-H. Yang, M. Yu, D.-L. Kwong, T. Zelevinsky, M. Jarrahi, and C. W. Wong, *Phys. Rev. X* **7**, 041002 (2017).
- G. Lin, R. Martinenghi, S. Diallo, K. Saleh, A. Coillet, and Y. K. Chembo, *Appl. Opt.* **54**, 2407 (2015).
- C. Bao, P. Liao, A. Kordts, L. Zhang, M. Karpov, M. H. Pfeiffer, Y. Cao, Y. Yan, A. Almain, G. Xie, A. Mohajerin-Ariaei, L. Li, M. Ziyadi, S. R. Wilkinson, M. Tur, T. J. Kippenberg, and A. E. Willner, *Opt. Lett.* **42**, 595 (2017).
- G. Lin, S. Diallo, R. Henriet, M. Jacquot, and Y. K. Chembo, *Opt. Lett.* **39**, 6009 (2014).
- F. Orucevic, V. Lefèvre-Seguin, and J. Hare, *Opt. Express* **15**, 13624 (2007).
- G. Lin, Y. Candela, O. Tillement, Z. Cai, V. Lefèvre-Seguin, and J. Hare, *Opt. Lett.* **37**, 5193 (2012).
- S. Diallo, G. Lin, and Y. K. Chembo, *Opt. Lett.* **40**, 3834 (2015).
- G. Lin and Y. K. Chembo, *Opt. Express* **23**, 1594 (2015).
- P. Parra-Rivas, D. Gomila, L. Gelens, and E. Knobloch, *Phys. Rev. E* **98**, 042212 (2018).
- Z. Qi, S. Wang, J. Jaramillo-Villegas, M. Qi, A. M. Weiner, G. D'Aguanno, T. F. Carruthers, and C. R. Menyuk, *Optica* **6**, 1220 (2019).
- A. Coillet, Z. Qi, I. V. Balakireva, G. Lin, C. R. Menyuk, and Y. K. Chembo, *Opt. Lett.* **44**, 3078 (2019).
- Y. K. Chembo, A. Coillet, G. Lin, P. Colet, and D. Gomila, *Chaos: An Interdiscip. J. Nonlinear Sci.* **30**, 083146 (2020).
- G. Lin, S. Diallo, J. M. Dudley, and Y. K. Chembo, *Opt. Express* **24**, 14880 (2016).